Journal of Catalysis 395 (2021) 1–9

Contents lists available at ScienceDirect

Journal of Catalysis

journal homepage: www.elsevier.com/locate/jcat

Role of silver species in H_2-NH_3-SCR of NO*x* over Ag/Al_2O_3 catalysts: *Operando* spectroscopy and DFT calculations

Guangyan Xu [a], Honghong Wang [a], Yunbo Yu [a,b,c,*], Hong He [a,b,c,*]

[a] State Key Joint Laboratory of Environment Simulation and Pollution Control, Research Center for Eco-Environmental Sciences, Chinese Academy of Sciences, Beijing 100085, China
[b] Center for Excellence in Regional Atmospheric Environment, Institute of Urban Environment, Chinese Academy of Sciences, Xiamen 361021, China
[c] University of Chinese Academy of Sciences, Beijing 100049, China

ARTICLE INFO

Article history:
Received 3 October 2020
Revised 16 December 2020
Accepted 22 December 2020
Available online 31 December 2020

Keywords:
NO*x*
H_2-NH_3-SCR
Ag/Al_2O_3
Operando DRIFTS-MS
Operando DR-UV–Vis
DFT calculations

ABSTRACT

The role of silver species in the H_2-assisted NH_3 selective catalytic reduction of NO*x* (H_2-NH_3-SCR) over Ag/Al_2O_3 catalysts was investigated by operando spectroscopy (DRIFTS-MS and DR-UV–Vis) and Density Functional Theory (DFT) calculation. UV–Vis analysis showed that several kinds of silver species were present on the Ag/Al_2O_3, including dispersed silver cations, partially oxidized silver clusters, metallic silver clusters, and silver nanoparticles. Operando DRIFTS-MS experiments showed that the reduction of NO*x* was dependent on the formation rate of nitrates, which was closely related to the silver content, H_2 concentration, and reaction temperature. Notably, operando DR-UV–Vis experiments unambiguously confirmed that the metallic silver clusters were the active sites for nitrates formation, and the reduction of silver nitrates was much slower than NO oxidation. DFT calculations further revealed that reducing silver nitrates required higher energy barriers than NO oxidation, while H_2 dissociation could occur on metallic silver clusters with a moderate energy barrier. In conclusion, metallic silver clusters contributed to the formation of nitrates and H_2 dissociation, and the reduction of silver nitrates was the rate-determining step in the overall H_2-NH_3-SCR reaction.

1. Introduction

NO*x* emission from vehicle exhaust has caused various environmental problems, including acid rain, photochemical smog, and haze [1]. Selective catalytic reduction (SCR) is a commercial technique for eliminating NO*x* from vehicles, especially heavy-duty diesel vehicles (HDDVs) [2]. Generally, ammonia is used as the reductant for NO*x* reduction (NH_3-SCR) with the assistance of V-based oxide or Cu-based zeolite catalysts [3–6]. In addition to NH_3-SCR, the hydrocarbon-SCR technique has unique advantages by employing on-board diesel to reduce NO*x* [7–9]. Ag/Al_2O_3 catalysts have been widely investigated in hydrocarbon-SCR due to their high efficiency and selectivity [7,9]. Besides, the addition of a trace of H_2 dramatically enhances the performance of Ag/Al_2O_3 in hydrocarbon-SCR [10–13]. Such an H_2 effect is also beneficial for NH_3-SCR on this catalyst, which is virtually inert in the absence of H_2 [14–16].

After the discovery of the anomalous H_2 effect on the NH_3-SCR reaction, several researchers devoted to studying the mechanism and practical application of this catalytic system [15–28]. Kondratenko et al. [15,17] studied the mechanism of H_2-NH_3-SCR using a TAP reactor and proposed that H_2 helps to reduce oxidized silver. Shimizu et al. [16,18] found that H_2 addition promoted superoxide ion formation, which was proposed to be an essential intermediate in this reaction. Doronkin et al. [19,25] suggested that both silver species and alumina were necessary components for the H_2-NH_3-SCR reaction. Olsson et al. [23,24] suggested that H_2 enhanced the conversion of nitrites and nitrates and free silver from single oxygen atoms. Besides, Fogel et al. [20,21,26] investigated this catalytic system's sulfur tolerance and further demonstrated its efficiency in engine-bench tests under harsh conditions. However, further improvement is required for the practical application of this H_2-NH_3-SCR system, and a fundamental understanding of the reaction mechanism is beneficial for its improvement.

Recently, we systematically investigated the reaction pathway of H_2-NH_3-SCR by kinetics and DRIFTS experiments [29]. It was found that this reaction obeyed the Langmuir-Hinshelwood mechanism. Notably, the bridging and bidentate nitrates reacted with the B_{NH_3} species (NH_3 adsorbs on Brønsted acid sites) and then produced nitrogen. Subsequently, the Brønsted acid sites could be recovered by H_2 dissociation. Based on the kinetic studies and

* Corresponding authors at: P.O. Box 2871, 18 Shuangqing Road, Haidian District, Beijing 100085, China.
E-mail addresses: ybyu@rcees.ac.cn (Y. Yu), honghe@rcees.ac.cn (H. He).

https://doi.org/10.1016/j.jcat.2020.12.025
0021-9517/

DRIFTS experiments, it was proposed that the rate-determining step should involve the generation of nitrates. The overall equation was summarized as: $2NO + 2NH_3 + 2O_2 + 3H_2 = 2\ N_2 + 6H_2O$. During this reaction, silver species played important roles in the generation of nitrates and the recovery of Brønsted acid sites. However, the roles of different silver species, such as dispersed silver cations, oxidized silver clusters, and metallic silver species in NO oxidation and H_2 dissociation, have not been demonstrated.

Hence, in the present work, Ag/Al_2O_3 catalysts containing various silver species were synthesized by impregnating Al_2O_3 with different silver amounts. Afterward, the roles of different silver species in H_2-NH_3-SCR were investigated by operando spectroscopy (DRIFTS-MS and DR-UV–Vis) and DFT calculations, which are important technologies for studying the reaction mechanism [30,31]. Operando DRIFTS-MS revealed that N_2 formation was closely related to nitrate species' generation, dependent on the silver content and reaction temperature. Notably, operando DR-UV–Vis unambiguously confirmed that metallic silver clusters were the active sites for NO oxidation and that the reduction of silver nitrates was the rate-determining step. DFT calculations further revealed that the reduction of silver nitrates had the highest energy barrier during the H_2-NH_3-SCR reaction. This work provides fundamental insight into the active sites on Ag/Al_2O_3 and can offer some advices for designing highly efficient deNO*x* catalysts.

2. Materials and methods

2.1. Catalyst preparation and catalytic test

Ag/Al_2O_3 catalysts with different silver loadings (0.5, 1, 2, and 3 wt%) were synthesized by an impregnation method [29,32]. Specifically, the silver nitrate solution was added into a boehmite (SASOL, SB-1) suspension with stirring. Then, the excess water was evaporated in a rotary evaporator. Subsequently, these samples were dried at 120 °C overnight and calcined in air at 600 °C for four hours. For comparison, γ-Al_2O_3 was prepared by the same procedure without impregnation with silver nitrate.

The catalytic activity tests were carried out in a fixed-bed reactor (i.d. 6 mm) [29,33]. The typical reaction gas consisted of 500 ppm NO, 500 ppm NH_3, 1500 ppm H_2, and 5% O_2 in N_2 balance (500 mL/min). A 150 mg sample (40–60 mesh) was used, corresponding to a GHSV of 150000 h^{-1}. The concentration of NO, NH_3, NO_2, and N_2O was monitored by an FTIR spectrometer (Nicolet iS 10). The NO*x* and NH_3 conversions were analyzed according to Eqs. (1) and (2).

$$NOxconversion = \frac{[NO + NO_2]_{in} - [NO + NO_2]_{out}}{[NO + NO_2]_{in}} \times 100\% \quad (1)$$

$$NH_3conversion = \frac{[NH_3]_{in} - [NH_3]_{out}}{[NH_3]_{in}} \times 100\% \quad (2)$$

To directly monitor the reaction products of N_2 and H_2O, another catalytic activity test (TPSR) was performed using online mass spectrometry (InProcess Instruments, GAM 200) as a detector. The tests were performed in a temperature-programmed mode in which the temperature was increased from 100 °C to 450 °C (2 °C/min). The gas composition was the same as in the above experiment except using Ar as balance (100 mL/min). The following *m*/*z* ratios were analyzed: 30 (NO), 2 (H_2), 28 (N_2), 18 (H_2O), 46 (NO_2), and 44 (N_2O). NH_3 (*m*/*z* = 17) was not monitored due to interference from the H_2O signal.

2.2. Catalyst characterization

BET analysis was performed on a physical adsorption instrument (Micromeritics, ASAP 2020) [32]. X-ray diffraction (XRD) measurements were conducted on a D8-ADVANCE (Bruker) diffractometer using Cu Kα radiation (40 kV, 40 mA) [32]. XPS analysis was conducted on a scanning X-ray microprobe (PHI Quantera) using C 1 s (284.8 eV) for calibration [34]. UV–Vis measurement was carried out on a UV–Vis spectrophotometer (LAMBDA 650, PerkinElmer) [29]. The signal was recorded from 800 nm to 190 nm at a resolution of 1 nm.

2.3. Operando DRIFTS-MS

Operando diffuse reflectance infrared Fourier transform spectroscopy experiments (DRIFTS-MS) were conducted on an FTIR spectrometer (Nicolet iS 50) equipped with a Harrick Praying Mantis Attachment (Model DRK-4) and a high-sensitivity mercury-cadmium-telluride (MCT/A) detector [29]. Powder samples were placed into a Harrick Scientific cell (HVC-DRP-5) controlled by a Harrick ATC Temperature Controller. The typical gas composition was the same as that in the TPSR experiment. The spectra were collected by accumulating 100 scans (4 cm^{-1}). The concentrations of NO and N_2 in the outlet gas were monitored by the mass spectrometry. Before each experiment, the sample was pretreated in 5% O_2/Ar at 400 °C for 30 min.

2.4. Operando DR-UV–Vis

Operando diffuse reflectance Ultraviolet–Visible experiments (DR-UV–Vis) were conducted on the above UV–Vis spectrophotometer. The above Harrick Praying Mantis Attachment and a Harrick Scientific cell were also used in the DR-UV–Vis experiments. The spectra were collected from 200 to 600 nm at a resolution of 5 nm. The DR-UV–Vis data were obtained by continuously measuring the absorbance at 350 nm at 1 point/s time-resolution. Except for using the N_2 balance, the reaction conditions were the same as in the DRIFTS-MS experiment.

2.5. DFT calculations

DFT calculations were performed using the Vienna Ab initio Simulation Package (VASP 5.4.1) [35]. According to previous works [32,36–38], the dehydrated surface of γ-Al_2O_3 (1 1 0) was modeled. Afterward, a catalyst structure of an Ag_8 cluster anchored on the γ-Al_2O_3 (1 1 0) surface was established and relaxed [39,40]. The reaction pathways and transition states were calculated based on the climbing image nudged elastic band (CI-NEB) method [41]. The electronic structure of Ag_8 cluster supported on Al_2O_3 was analyzed by density of states (DOS). Detailed information about the DFT calculations can be found in the supplementary materials.

3. Results and discussion

3.1. Catalytic performance

Unlike industrial catalysts, SCR catalysts need to operate over a wide temperature range under specific conditions [6,8]. Hence, the catalytic activity of Ag/Al_2O_3 catalysts in the H_2-NH_3-SCR was shown in the form of NO*x* conversion concerning the reaction temperature (Fig. 1). Al_2O_3 was almost entirely inactive for NO*x* reduction in this reaction. Impregnation with a low content of silver hardly affected the catalytic activity of the 0.5% Ag/Al_2O_3 for NO*x* reduction. In contrast, loading with 1 wt% silver significantly improved the deNO*x* activity of 1% Ag/Al_2O_3, which achieved about

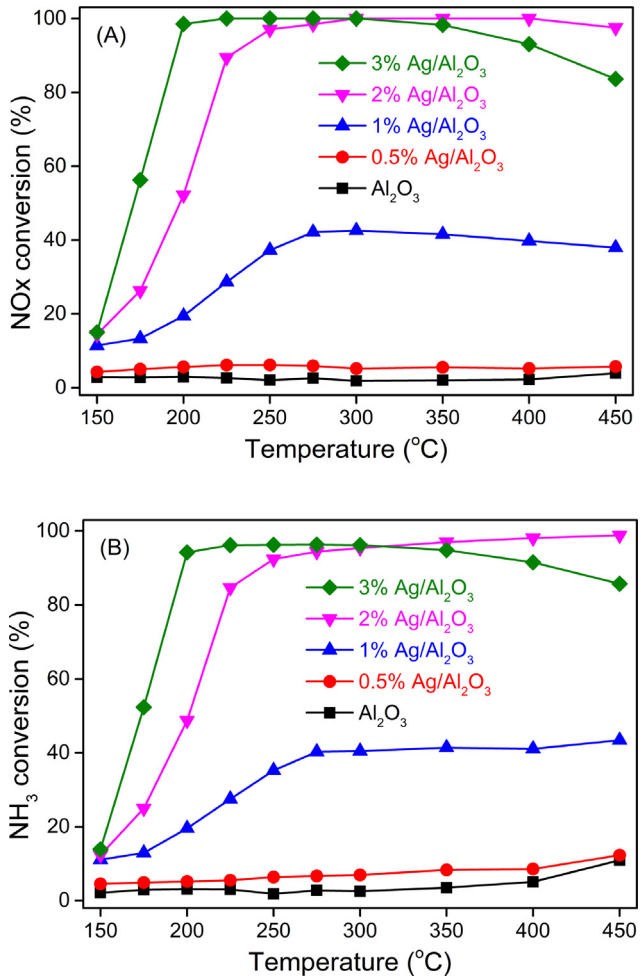

Fig. 1. The conversions of NO*x* (A) and NH_3 (B) during the H_2-NH_3-SCR on Ag/Al_2O_3 catalysts.

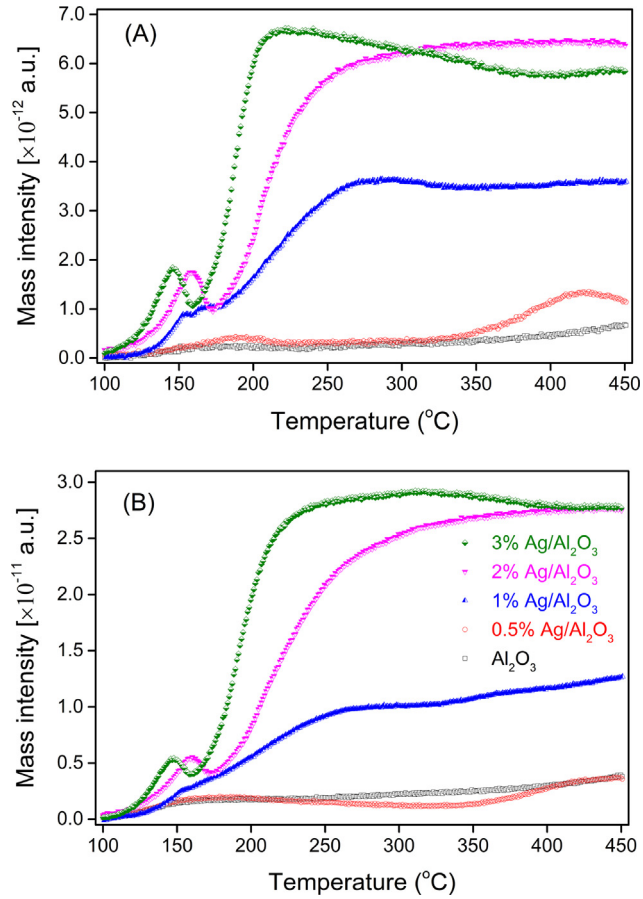

Fig. 2. The formation of (A) N_2 (m/z = 28) and (B) H_2O (m/z = 18) during the H_2-NH_3-SCR on Ag/Al_2O_3 catalysts.

40% NO*x* conversion at temperatures above 275 °C. Notably, 2% Ag/Al_2O_3 exhibited extremely high efficiency for NO*x* reduction at temperatures above 225 °C. Further increase in silver loading (3 wt%) could reduce the light-off temperature of NO*x* reduction at the cost of losing high-temperature activity to some extent, which might be due to non-selective oxidation of the reductant. Besides, the NH_3 conversion rate showed the same trend as the NO*x* conversion rate, revealing the occurrence of the standard SCR reaction. Moreover, the formation of N_2O in this reaction was negligible, revealing a high selectivity toward N_2.

The formation of N_2 and H_2O during the TPSR experiment of the H_2-NH_3-SCR reaction is shown in Fig. 2 and S1. Similarly, neither Al_2O_3 nor 0.5% Ag/Al_2O_3 were active for NO*x* reduction, while 2% Ag/Al_2O_3 and 3% Ag/Al_2O_3 could almost entirely reduce NO at temperatures above 225 °C. Notably, substantially all the NO reduced was converted to N_2 without the formation of byproducts of NO_2 or N_2O. Also, H_2 consumption followed a similar trend to NO*x* reduction, and the H_2O yield was about 4–4.5 times that of N_2, which was consistent with the theoretical value. The slight increase in NO concentration on 0.5% Ag/Al_2O_3 at 450 °C possibly originated from the direct oxidation of NH_3 (Fig. S1).

Interestingly, a narrow peak of NO*x* reduction was observed at about 150 °C on 2% Ag/Al_2O_3 and 3% Ag/Al_2O_3. A TPSR experiment of H_2 oxidation was performed on Ag/Al_2O_3 catalysts to investigate this phenomenon (Fig. S2). Al_2O_3 and 0.5% Ag/Al_2O_3 were completely inactive for H_2 oxidation, and 1% Ag/Al_2O_3 showed only slight catalytic oxidation of H_2 to produce H_2O at high temperatures. In contrast, the Ag/Al_2O_3 catalysts with high silver loadings (2 and 3 wt%) exhibited high H_2 oxidation efficiency at temperatures above 300 °C. It should be noted that the light-off temperature for H_2 oxidation on these samples was about 150 °C, which was consistent with the above NO*x* reduction peak. Therefore, this peak might originate from the rapid reduction of accumulated surface intermediates after H_2 activation at about 150 °C. During the H_2 oxidation, the formation of H_2O was slightly different from the theoretical value, which might be due to the influence of water condensation.

3.2. Characterization

The surface and structural properties of Ag/Al_2O_3 were investigated by BET and XRD (Fig. 3A and Table S1). Pure Al_2O_3 showed a BET surface area of 205 m^2/g and an average pore size of 8.09 nm. Ag/Al_2O_3 catalysts showed substantially the same BET surface areas as the Al_2O_3, while the average pore sizes were only slightly smaller than the latter. Nevertheless, the 0.5% Ag/Al_2O_3 sample exhibited a slightly larger BET surface area (232 m^2/g), which might be due to the blockage of pore tunnels by dispersed silver species. XRD analysis showed that Ag/Al_2O_3 catalysts contain the same crystal phases as the pure Al_2O_3 (γ-Al_2O_3), and no silver phase was observed (Fig. 3A), which was consistent with previous literature [42]. Hence, the impregnation with silver hardly affected the surface and structural properties of the Al_2O_3 support.

XPS analysis (Fig. 3B) showed that the surface silver concentration on the Ag/Al_2O_3 catalysts increased in proportion with the sil-

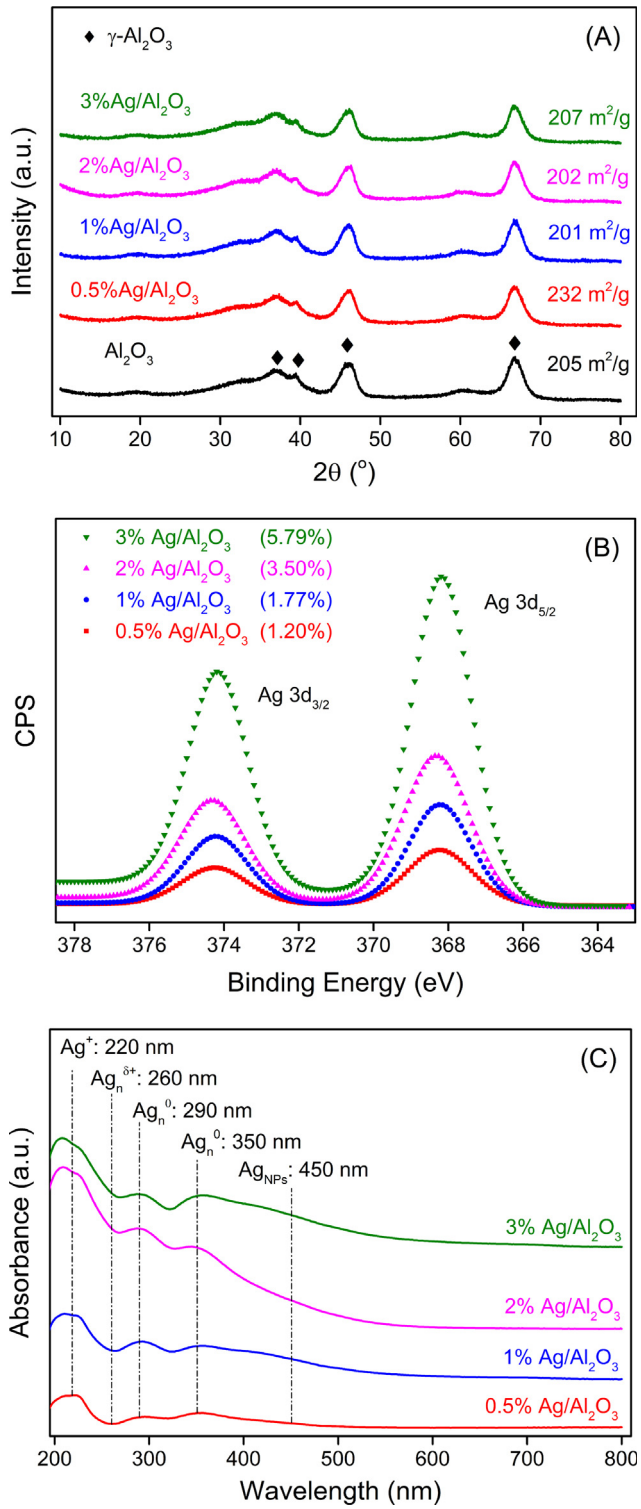

Fig. 3. XRD patterns (A), XPS spectra (B), and UV–Vis spectra (C) of Ag/Al_2O_3 catalysts.

ver content. The higher silver concentration on the surface could be attributed to the anchoring of silver species on the Al_2O_3 surface during impregnation. Due to the subtle differences in the binding energy of different silver species, XPS results could not provide further information about silver species' valence state. Therefore, UV–Vis analysis was carried out to identify the silver species' valence state (Fig. 3C). Al_2O_3 was employed as the reference to eliminate effects from absorption by the support. There were five absorption peaks observed on these samples, which could be attributed to dispersed silver cations (Ag^+, 220 nm), partially oxidized silver clusters ($Ag_n^{\delta+}$, 260 nm), metallic silver clusters (Ag_n^0, 290 and 350 nm), and silver nanoparticles (Ag_{NPs}, 450 nm) [42–45]. The dispersed silver cations were predominant on all silver catalysts, whereas only a trace amount of silver clusters ($Ag_n^{\delta+}$ and Ag_n^0) were observed on the sample with extremely low silver loading (0.5 wt %). On 1% Ag/Al_2O_3, the number of silver clusters was higher than for 0.5% Ag/Al_2O_3. It should be highlighted that the silver clusters were relatively abundant on the samples with higher silver content (2 and 3 wt%). Besides, silver nanoparticles were observed on 3% Ag/Al_2O_3, possibly due to the agglomeration of a high density of silver species. Moreover, silver species was hardly observed in HR-TEM images of 2% Ag/Al_2O_3 catalysts (not shown), further revealing the well dispersion of silver species. Recently, dispersed silver atoms and silver clusters have been directly observed on a 2 wt% Ag/Al_2O_3 by HR-HAADF/STEM [46]. As the 0.5% Ag/Al_2O_3 and 2% Ag/Al_2O_3 samples showed remarkable differences in the catalyst parameters and catalytic activity, this study will mainly focus on these two samples in later sections.

3.3. Operando DRIFTS-MS

Operando DRIFTS-MS experiments of H_2-NH_3-SCR were performed on Ag/Al_2O_3 to investigate the surface reaction and gaseous products (Fig. 4). There were several intermediates observed, such

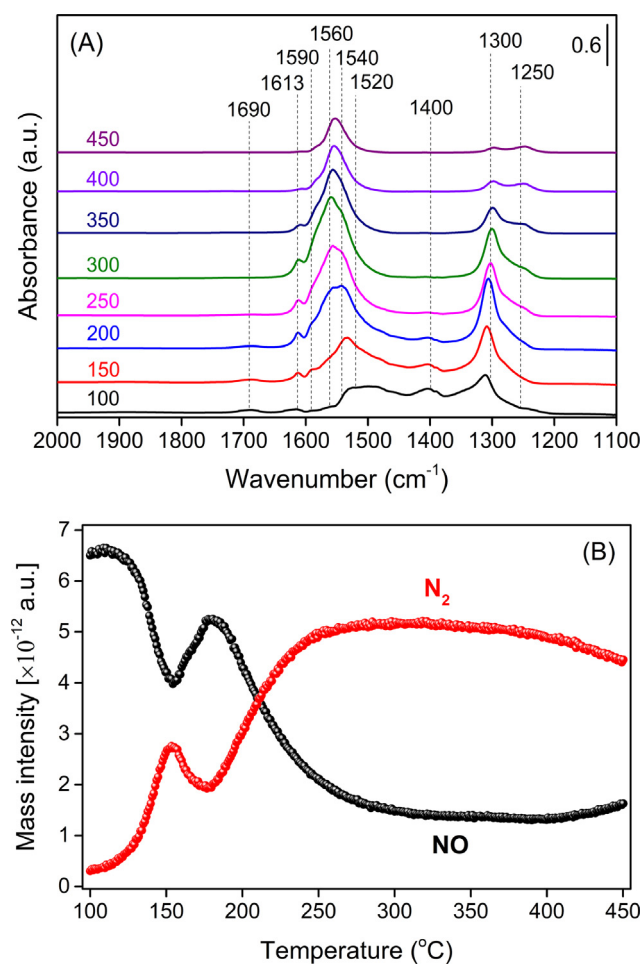

Fig. 4. Operando DRIFTS-MS experiment of H_2-NH_3-SCR on the 2%Ag/Al_2O_3 catalyst. The reaction conditions were the same as those of the TPSR experiment (Fig. 2).

as B_{NH_3} species (1400 and 1690 cm^{-1}), bridging nitrate (1613 cm^{-1}), bidentate nitrate (1590 and 1250 cm^{-1}), and monodentate nitrates (1560, 1540, 1520, and 1300 cm^{-1}) [19,24,29]. Notably, the formation of N_2 was approximately the same as in the TPSR experiment (Fig. 2), revealing that the DRIFTS experiment was conducted under operando conditions (Fig. 4B). The slightly lower N_2 yield might be due to the escape of reactants in the bypass. As the generation of nitrates is critical for the H_2-NH_3-SCR reaction [29], the study will mainly focus on nitrate formation.

The catalytic oxidation of NO on Ag/Al_2O_3 was investigated at elevated temperatures (Fig. 5). The adsorption of intermediates was recorded in the first few minutes for the consideration of kinetic regions [29]. Several nitrate species were observed on these samples, including bridging nitrate, bidentate nitrate, and monodentate nitrate. The Ag/Al_2O_3 samples with low silver contents (0.5 and 1 wt%) exhibited low NO oxidation activity at 200 °C, while the 1% Ag/Al_2O_3 was slightly better than 0.5% Ag/Al_2O_3 (inset in Fig. 5A). In contrast, the high-loading samples (2 and 3 wt%) showed an excellent ability for NO oxidation, especially 3% Ag/Al_2O_3. Furthermore, a similar experiment was performed on 2% Ag/Al_2O_3 at elevated temperatures (Fig. 5B). At 100 °C, this sample was entirely inactive for NO oxidation, while its catalytic activity was gradually enhanced at elevated temperatures. Therefore, the oxidation of NO on Ag/Al_2O_3 was closely related to the silver content and reaction temperature, which was in good agreement with the NO*x* reduction activity.

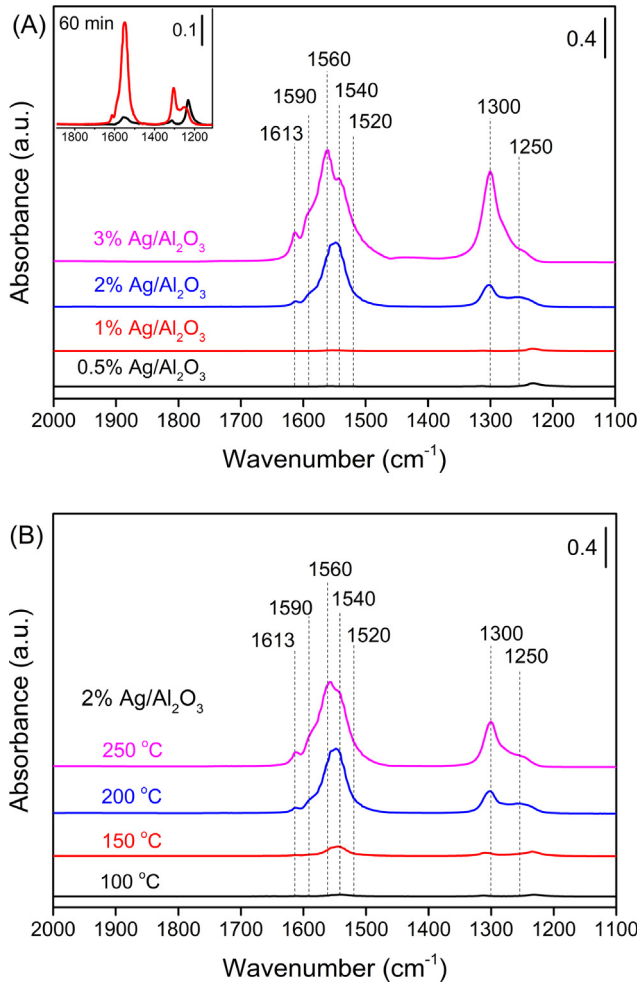

Fig. 5. Operando DRIFTS of nitrates formation on Ag/Al_2O_3 catalysts with different silver loadings at 200 °C (A) and the 2% Ag/Al_2O_3 at elevated temperatures (B) after exposure to a flow of $H_2/NO/O_2/Ar$ for 7 min. The inset in (A) shows the nitrates adsorption on 0.5% Ag/Al_2O_3 (black) and 1% Ag/Al_2O_3 (red) after exposure for 60 min.

Furthermore, a step-response experiment was performed to investigate the surface intermediates and gaseous products occurring during H_2-NH_3-SCR on Ag/Al_2O_3 (Fig. 6 and S3). After pretreatment, Ag/Al_2O_3 catalysts were successively exposed to $NO/NH_3/O_2$ (black), $H_2/NO/NH_3/O_2$ (red), $H_2/NO/O_2$ (blue), $H_2/NO/NH_3/O_2$ (magenta), and $H_2/NH_3/O_2$ (olive), respectively. Without H_2, the 2% Ag/Al_2O_3 catalyst could not reduce NO*x*, with little adsorbed species on the surface (Fig. 6A and 6B). The addition of 1500 ppm H_2 rapidly and significantly increased the number of surface intermediates and the gaseous product of N_2. After the removal of NH_3, both the adsorbed B_{NH_3} species and gaseous N_2 formation gradually decreased within several minutes. At the same time, the bridging and bidentate nitrates gradually increased after the consumption of B_{NH_3} species (Fig. S3B). After the introduction of NH_3, the N_2 yield was rapidly recovered. In the last step, NO was removed from the gas mixture, resulting in the gradual consumption of nitrate species. Interestingly, the N_2 formation suddenly decreased by half, and then gradually decreased within 60 min. Meanwhile, the bridging and bidentate nitrates were gradually consumed (Fig. S3C) during the above process. It was speculated that the NH_3 species preferentially reacted with the freshly produced nitrates adsorbed at the Ag-O-Al interface rather than with the nitrates stored on the Al_2O_3 surface.

On 0.5% Ag/Al_2O_3, however, H_2 addition only slightly enhanced the formation of monodentate nitrate as well as the gaseous product of N_2 (Fig. 6C and 6D). After removing NH_3, the formation of N_2 was gradually reduced, accompanied by a slight increase in the adsorption of nitrates. Notably, the adsorption of reactive nitrates on this sample was negligible compared to that on 2% Ag/Al_2O_3. Then, the reaction was resumed by introducing NH_3, and the generation of N_2 gradually increased within 25 min. Finally, the reaction involved N_2 formation was rapidly stopped once NO was removed, further revealing that nitrate formation was involved in the rate-determining step in this reaction.

3.4. Operando DR-UV–Vis

Silver species play a critical role in the generation of nitrate species, an essential step in H_2-NH_3-SCR. Hence, an operando DR-UV–Vis experiment was performed on the Ag/Al_2O_3 catalysts to identify the dynamic state of silver species during nitrate formation (Fig. 7). After pretreatment, these samples were cooled to 200 °C, and then a spectrum was collected for reference. These samples were then sequentially exposed to $H_2/O_2/N_2$, $NO/O_2/N_2$, $H_2/O_2/N_2$, and $NO/O_2/N_2$, respectively. On 2% Ag/Al_2O_3 (Fig. 7A), H_2 addition reduced the silver species and increased the number of metallic silver clusters (290 and 350 nm). However, after exposure to NO + O_2, the metallic silver clusters were rapidly oxidized, which might be due to the formation of silver nitrate. Subsequently, the oxidized silver species could be further reduced by H_2, followed by reoxidation in the presence of NO + O_2. Therefore, a complete redox cycle of silver species (mainly silver clusters) was confirmed during nitrate formation. In contrast, the dispersed silver cations (220 nm) showed little change during the above procedures. In contrast, on 0.5% Ag/Al_2O_3, H_2 addition hardly changed the valence state of silver species (Fig. 7B). Instead, exposure to NO + O_2 appreciably increased the number of silver cations (220 nm), which could be attributed to the generation of dispersed silver nitrate. Subsequently, H_2 reduction only slightly decreased the number of silver cations, which was subsequently increased in a flow of NO + O_2. In the above procedures, silver clusters exhibited a minor response to the gas switching, probably due to these species' low content (Fig. 3C). Obviously, the silver species on 0.5% Ag/Al_2O_3

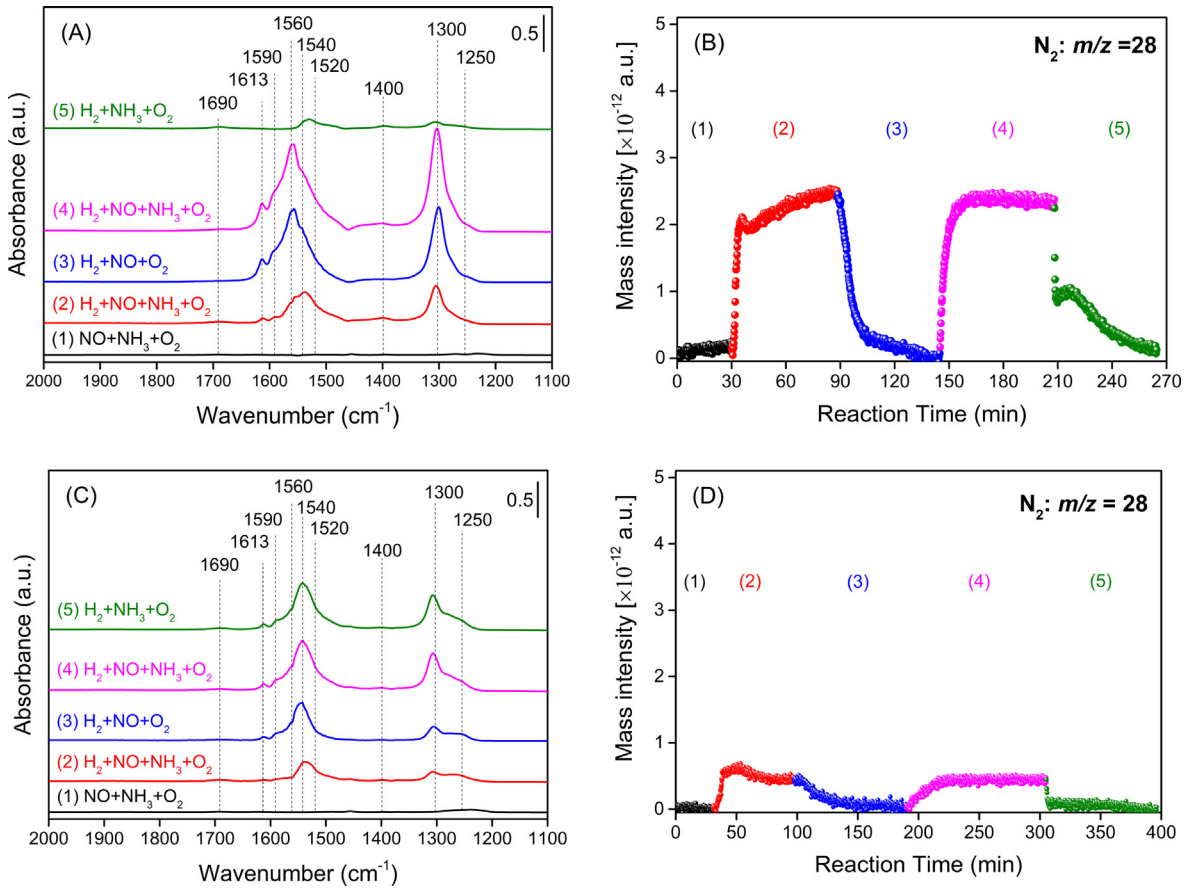

Fig. 6. Operando DRIFTS spectra of adsorbed species on 2% Ag/Al_2O_3 (A) and 0.5% Ag/Al_2O_3 (C) under different conditions at 200 °C and dynamic change of the MS signal of N_2 during gas switching on 2% Ag/Al_2O_3 (B) and 0.5% Ag/Al_2O_3 (D). These samples were successively exposed to (1) $NO/NH_3/O_2$ (black), (2) $H_2/NO/NH_3/O_2$ (red), (3) $H_2/NO/O_2$ (blue), (4) $H_2/NO/NH_3/O_2$ (magenta), and (5) $H_2/NH_3/O_2$ (olive), respectively.

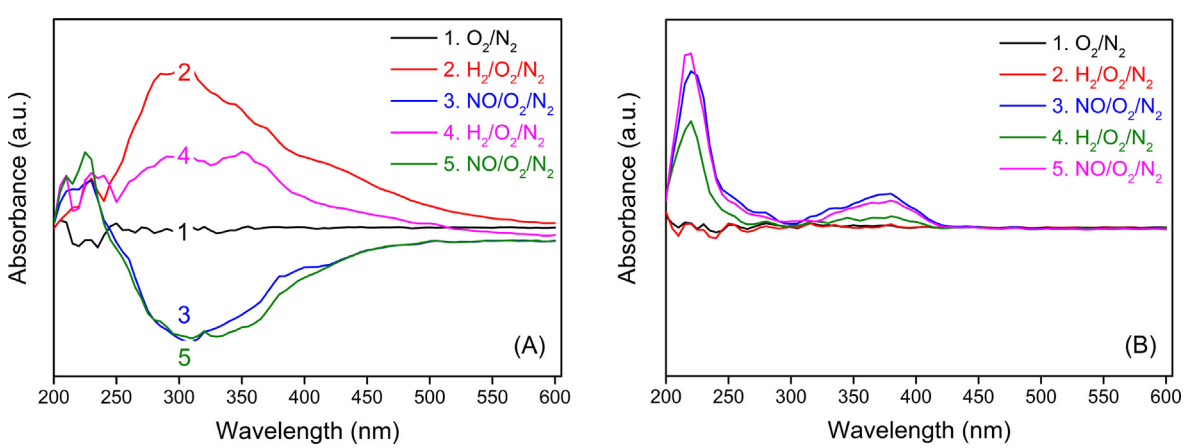

Fig. 7. Operando DR-UV–Vis spectra of 2% Ag/Al_2O_3 (A) and 0.5% Ag/Al_2O_3 (B) under different conditions at 200 °C. These samples were sequentially exposed to O_2/N_2, $H_2/O_2/N_2$, $NO/O_2/N_2$, $H_2/O_2/N_2$, and $NO/O_2/N_2$, respectively, each step lasting for 12 min.

exhibited less change during nitrate formation than the 2% Ag/Al_2O_3.

As metallic silver clusters were found to play an essential role in nitrate formation, a step-response experiment was performed on the Ag/Al_2O_3 catalysts to investigate the dynamic changes of metallic silver clusters during NO oxidation (Fig. 8). After pretreatment and cooling to 200 °C, these samples were successively exposed to $H_2/O_2/N_2$, O_2/N_2, $H_2/O_2/N_2$, $NO/O_2/N_2$, $H_2/O_2/N_2$, and O_2/N_2, respectively. First, H_2 reduced the oxidized silver and thus increased the amount of metallic silver clusters, which were re-oxidized after the removal of H_2. Once the reaction gas was switched from $H_2/O_2/N_2$ to $NO/O_2/N_2$, the metallic silver species were rapidly oxidized and possibly produced silver nitrate species. Afterward, these oxidized silver species were further reduced to metallic silver species in $H_2/O_2/N_2$, and finally re-oxidized in O_2/N_2, thus completing the redox cycle of silver species. During the above procedures, in the absence of NO, the reduction of silver species was much faster than their subsequent oxidation. However,

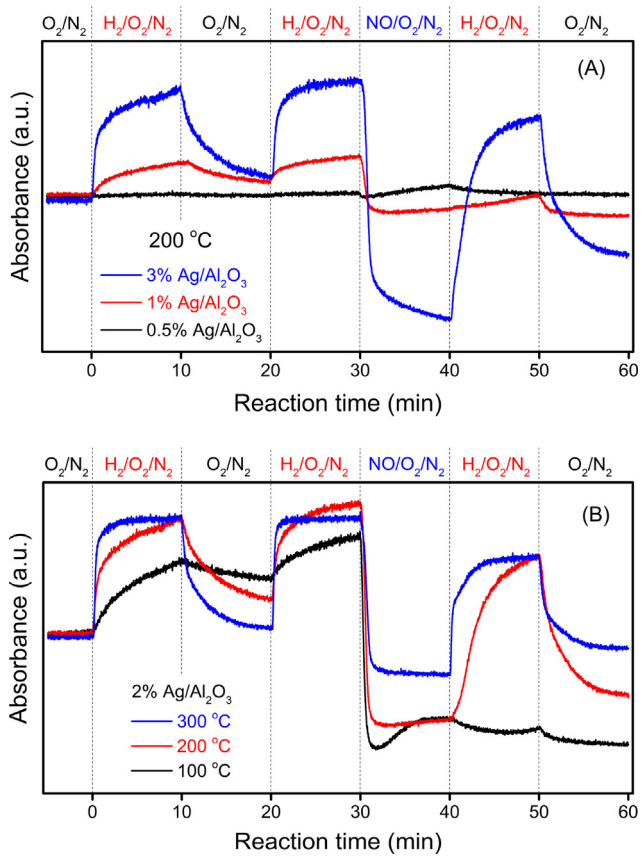

Fig. 8. Dynamic change of metallic Ag clusters (350 nm) on Ag/Al_2O_3 catalysts at 200 °C (A) and 2%Ag/Al_2O_3 at different temperatures (B) during gas switching. These samples were successively exposed to $H_2/O_2/N_2$, O_2/N_2, $H_2/O_2/N_2$, $NO/O_2/N_2$, $H_2/O_2/N_2$, and O_2/N_2, respectively.

the addition of NO remarkably accelerated the oxidation of metallic silver clusters, possibly due to silver nitrates' formation. More importantly, the reduction of oxidized silver clusters became more difficult after exposure to NO, indicating that silver nitrate formation suppressed the reduction of these silver species. Consequently, the silver reduction was much slower than their oxidation after exposure to NO. Meanwhile, the redox rate of Ag/Al_2O_3 with higher silver loading was much faster than those with lower silver contents. In particular, the silver clusters on 0.5% Ag/Al_2O_3 exhibited little change during gas switching, which might be due to the low content or the low reactivity.

The same experiment was further performed on 2% Ag/Al_2O_3 at 100 °C and 300 °C. Generally, both the reduction and oxidation of silver clusters were gradually enhanced as the reaction temperature increased. Similarly, the reduction of silver clusters was faster than its re-oxidation in the absence of NO at different temperatures. However, NO greatly enhanced the oxidation of metallic silver clusters regardless of the reaction temperature. In contrast, reducing silver nitrates was so strongly temperature-dependent that it hardly occurred at low temperature (100 °C). The reduction rate of silver species was also closely related to the H_2 concentration, the increase of which significantly increased the reduction rate (Fig. S4). Hence, it was unambiguously confirmed that the reduction of oxidized silver clusters (silver nitrates) was the rate-determining step during nitrate formation.

3.5. DFT calculations

DFT calculations were conducted to study further the energy barriers for nitrate formation and H_2 dissociation on the Ag/Al_2O_3 catalysts. As silver clusters were the main active sites for nitrates formation, a catalyst structure of an Ag_8 cluster anchored on γ-Al_2O_3 (1 1 0) surface was established (Fig. S5). DOS calculations showed that the Ag_8 cluster supported on Al_2O_3 were electron-deficient metallic silver (Fig. S6), possibly due to the interaction with Al_2O_3 support. On the Ag_8-Al_2O_3 surface, NO was much inclined to react with O_2 to form silver nitrates (Fig. 9A), with a shallow energy barrier (0.01 eV). It was highly consistent with the operando DR-UV–Vis result that this reaction could occur quickly even at a low temperature of 100 °C. In contrast, silver nitrates' reduction had a higher energy barrier (0.88 eV), revealing that silver reduction was slower than their oxidation (Fig. 9B). Moreover, the dissociation of H_2 on Ag clusters had a moderate energy barrier of 0.55 eV (Fig. 9C), indicating that this reaction could occur at a higher rate. Consistent with the operando DR-UV–Vis results, DFT calculations further confirmed that NO oxidation mainly occurs on the silver clusters and that the reduction of silver nitrate is the rate-determining step of this reaction. Besides, the energy barrier for silver nitrates' reduction (0.88 eV, 84.8 kJ/mol) obtained by DFT calculations was higher than the activation energy for overall H_2-NH_3-SCR reaction (41.6 kJ/mol) obtained in kinetic experiments [29], possibly due to different experimental settings.

3.6. Active sites on the Ag/Al_2O_3 catalysts

As demonstrated in our previous work [29], the H_2-NH_3-SCR reaction started with NO oxidation to yield nitrates, which further reacted with B_{NH_3} species to generate N_2. Subsequently, the Brønsted acid sites were restored by H_2 dissociation. Based on the kinetic and DRIFTS studies, it was proposed that nitrate formation was involved in the rate-determining step of H_2-NH_3-SCR over Ag/Al_2O_3. In the above processes, silver species served as the active sites for nitrate formation and H_2 dissociation.

According to UV–Vis analysis, dispersed silver cations, partially oxidized silver clusters, metallic silver clusters, and silver nanoparticles were observed on Ag/Al_2O_3. Dispersed silver cations were predominant on the Ag/Al_2O_3 sample with low silver content (0.5 wt%). Meanwhile, a further increase in silver loading proportionally increased the number of silver clusters on Ag/Al_2O_3. In particular, silver nanoparticles started to emerge on 3% Ag/Al_2O_3 due to the aggregation of high-density silver species. Besides, silver impregnation showed a negligible influence on the surface and structural properties of the Al_2O_3 support.

During the formation of nitrates on Ag/Al_2O_3, metallic silver species catalytically oxidized NO to produce silver nitrate. Afterward, H_2 reduced the silver nitrate and forced the nitrates to transfer to the Al_2O_3 surface, thereby restoring the metallic silver species. Subsequently, the nitrate species reacted with NH_3 adsorbed on Brønsted acid sites to produce N_2 and H_2O. Operando DR-UV–Vis revealed that metallic silver clusters showed high efficiency for NO oxidation to produce silver nitrate, which was further confirmed by DFT calculations. Incidentally, as the small Ag_8 cluster supported on Al_2O_3 were electron-deficient metallic silver, the calculations may be slightly different from actual conditions. The reduction of silver nitrates by H_2 required a higher energy barrier than its oxidation, resulting in a slower reduction rate. Notably, the reduction rate was dependent on the silver loading, reaction temperature, and H_2 concentration. In contrast, the dispersed silver cations exhibited low efficiency for NO oxidation to produce silver nitrate. Hence, metallic silver clusters were the main active sites for nitrate formation, while the reduction of silver nitrates was the rate-determining step in this reaction.

Consequently, the 0.5% Ag/Al_2O_3 sample containing highly dispersed silver cations was inactive for NO oxidation to yield

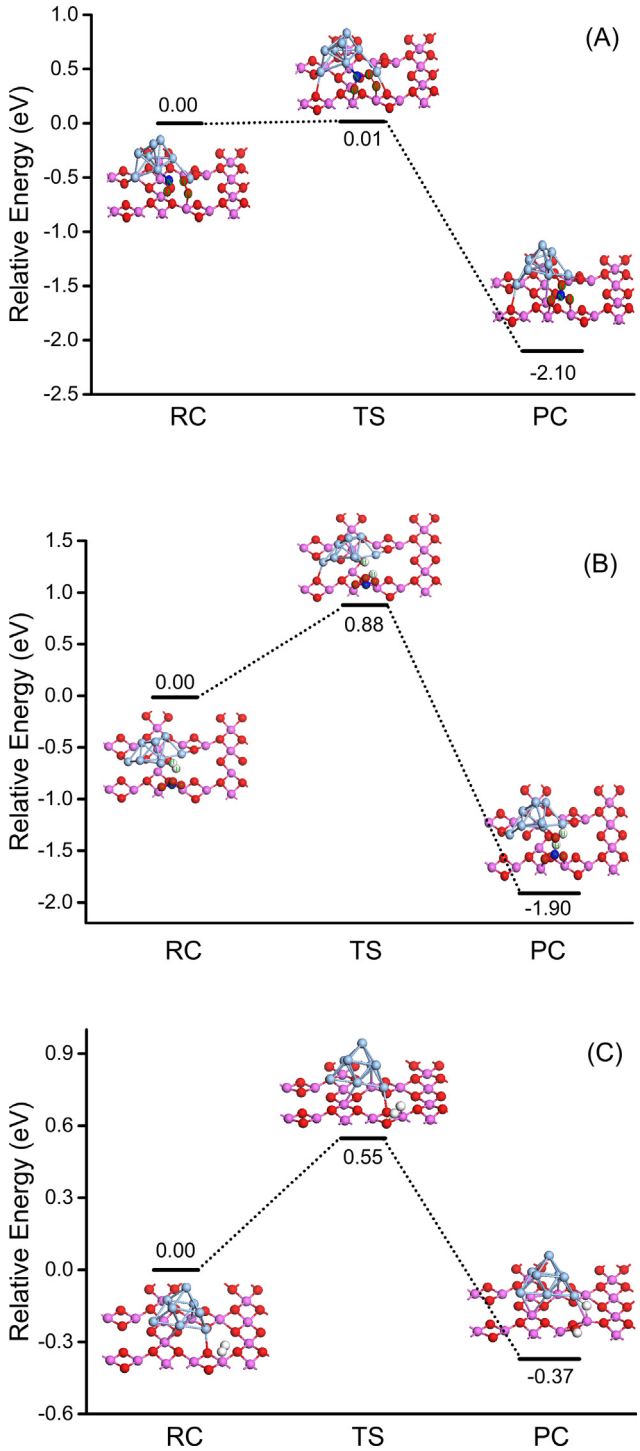

Fig. 9. Energy profiles of the oxidation of NO + O_2 (A), the reduction of silver nitrates (B), and H_2 dissociation (C) on the Ag_8-Al_2O_3 surface as well as the optimized geometries of the reactant, transition state, and product. Light blue, pink, red, blue, and white circles denote Ag, Al, O, N, and H atoms, respectively.

nitrates, which resulted in low activity for NO*x* reduction. In contrast, the increase in the silver loading proportionally increased the number of silver clusters on Ag/Al_2O_3, thus gradually enhancing the formation of nitrates, which ultimately contributed to the better deNO*x* activity on these samples. Furthermore, the increase in the reaction temperature and H_2 concentration could also enhance the reduction rate of silver nitrate, which further improved the formation of nitrates and the NO*x* conversion. Besides, the silver nanoparticles present on the 3% Ag/Al_2O_3 catalyst, on the one hand, reduced the light-off temperature of NO*x* reduction and, on the other hand, caused non-selective oxidation of the reductant at high temperature.

Another role of the silver species was to dissociate H_2 to generate acidic H atoms, which further helped restore the Brønsted acid sites for NH_3 adsorption. Besides, H_2 also contributed to the activation of NH_3 during NH_3-SCO over Ag/Al_2O_3 [29]. DFT calculations revealed that H_2 could dissociate on the silver clusters with a lower energy barrier than the reduction of silver nitrates. Besides, the concentration of gaseous NH_3 hardly affected the overall reaction rate of the H_2-NH_3-SCR [29], demonstrating that the restoration of Brønsted acid sites was not involved in the rate-determining step. In summary, the catalytic activity of Ag/Al_2O_3 in the H_2-NH_3-SCR was dependent on the formation rate of nitrate species, which was closely related to the silver loading, reaction temperature, and H_2 concentration. The present work combined operando spectroscopy and DFT calculations to systematically investigate the dynamic change of active sites on Ag/Al_2O_3 and reactive intermediates in H_2-NH_3-SCR, and such a combined method could be beneficial for the investigation of other catalytic systems.

4. Conclusions

Several kinds of silver species were present on the Ag/Al_2O_3 catalysts, including dispersed silver cations, partially oxidized silver clusters, metallic silver clusters, and silver nanoparticles. The silver species on Ag/Al_2O_3 contributed to the catalytic oxidation of NO to generate nitrates and H_2 dissociation to restore the Brønsted acid sites. Notably, operando DR-UV–VIS unambiguously confirmed that metallic silver clusters were the active sites for NO oxidation to produce nitrate species, and the reduction of silver nitrates was much slower than NO oxidation. DFT calculations further confirmed that reducing silver nitrates required higher energy barriers than NO oxidation, while H_2 dissociation could occur on metallic silver clusters with a moderate energy barrier. Hence, the reduction of silver nitrates, which was closely related to reaction temperature and H_2 concentration, was the rate-determining step in the overall H_2-NH_3-SCR reaction.

Declaration of Competing Interest

The authors declare that they have no known competing financial interests or personal relationships that could have appeared to influence the work reported in this paper.

Acknowledgments

This work was supported by the National Key R&D Program of China (2017YFC0211105), the National Natural Science Foundation of China (21906171, 21673277, and 21637005), the K.C. Wong.

Education Foundation, and the Strategic Priority Research Program of the Chinese Academy of Sciences (XDA23010200).

Appendix A. Supplementary data

Supplementary data to this article can be found online at https://doi.org/10.1016/j.jcat.2020.12.025.

References

[1] A. Richter, J.P. Burrows, H. Nüß, C. Granier, U. Niemeier, Increase in tropospheric nitrogen dioxide over China observed from space, Nature 437 (7055) (2005) 129–132.

[2] R.M. Heck, R.J. Farrauto, S.T. Gulati, Catalytic air pollution control: commercial technology, 3rd ed., Wiley, New York, 2009.

[3] G. Busca, L. Lietti, G. Ramis, F. Berti, Chemical and mechanistic aspects of the selective catalytic reduction of NOx by ammonia over oxide catalysts: A review, Appl. Catal. B: Environ. 18 (1998) 1–36.
[4] A.M. Beale, F. Gao, I. Lezcano-Gonzalez, C.H.F. Peden, J. Szanyi, Recent advances in automotive catalysis for NO x emission control by small-pore microporous materials, Chem. Soc. Rev. 44 (20) (2015) 7371–7405.
[5] L. Han, S. Cai, M. Gao, J.-Y. Hasegawa, P. Wang, J. Zhang, L. Shi, D. Zhang, Selective catalytic reduction of NOx with NH_3 by using novel catalysts: state of the art and future prospects, Chem. Rev. 119 (2019) 10916–10976.
[6] C.K. Lambert, Current state of the art and future needs for automotive exhaust catalysis, Nat Catal 2 (7) (2019) 554–557.
[7] R. Burch, J.P. Breen, F.C. Meunier, A review of the selective reduction of NOx with hydrocarbons under lean-burn conditions with non-zeolitic oxide and platinum group metal catalysts, Appl. Catal. B: Environ. 39 (4) (2002) 283–303.
[8] P. Granger, V.I. Parvulescu, Catalytic NOx abatement systems for mobile sources: From three-way to lean burn after-treatment technologies, Chem. Rev. 111 (2011) 3155–3207.
[9] H. He, Y.B. Yu, Selective catalytic reduction of NOx over Ag/Al_2O_3 catalyst: from reaction mechanism to diesel engine test, Catal. Today 100 (2005) 37–47.
[10] S. Satokawa, Enhancing the $NO/C_3H_8/O_2$ Reaction by Using H_2 over Ag/Al_2O_3 Catalysts under Lean-Exhaust Conditions, Chem. Lett. 29 (3) (2000) 294–295.
[11] S. Satokawa, J. Shibata, K.-I. Shimizu, A. Satsuma, T. Hattori, Promotion effect of H_2 on the low temperature activity of the selective reduction of NO by light hydrocarbons over Ag/Al_2O_3, Appl. Catal. B: Environ. 42 (2) (2003) 179–186.
[12] P. Sazama, L. Capek, H. Drobna, Z. Sobalik, J. Dedecek, K. Arve, B. Wichterlova, Enhancement of decane-SCR-NOx over Ag/alumina by hydrogen. Reaction kinetics and in situ FTIR and UV-vis study, J. Catal. 232 (2005) 302–317.
[13] K. Shimizu, J. Shibata, A. Satsuma, Kinetic and in situ infrared studies on SCR of NO with propane by silver-alumina catalyst: Role of H_2 on O_2 activation and retardation of nitrate poisoning, J. Catal. 239 (2006) 402–409.
[14] M. Richter, R. Fricke, R. Eckelt, Unusual Activity Enhancement of NO Conversion over Ag/Al_2O_3 by Using a Mixed NH_3/H_2 Reductant Under Lean Conditions, Catal. Letters 94 (1/2) (2004) 115–118.
[15] E.V. Kondratenko, V.A. Kondratenko, M. Richter, R. Fricke, Influence of O_2 and H_2 on NO reduction by NH_3 over Ag/Al_2O_3: A transient isotopic approach, J. Catal. 239 (2006) 23–33.
[16] K.-I. Shimizu, A. Satsuma, Reaction Mechanism of H_2-Promoted Selective Catalytic Reduction of NO with NH_3 over Ag/Al_2O_3, J. Phys. Chem. C 111 (5) (2007) 2259–2264.
[17] V.A. Kondratenko, U. Bentrup, M. Richter, T.W. Hansen, E.V. Kondratenko, Mechanistic aspects of N_2O and N_2 formation in NO reduction by NH_3 over Ag/Al_2O_3: The effect of O_2 and H_2, Appl. Catal. B: Environ. 84 (3–4) (2008) 497–504.
[18] K.-I. Shimizu, A. Satsuma, Hydrogen assisted urea-SCR and NH_3-SCR with silver–alumina as highly active and SO_2-tolerant de-NOx catalysis, Appl. Catal. B: Environ. 77 (1–2) (2007) 202–205.
[19] D.E. Doronkin, S. Fogel, S. Tamm, L. Olsson, T.S. Khan, T. Bligaard, P. Gabrielsson, S. Dahl, Study of the "Fast SCR"-like mechanism of H_2-assisted SCR of NOx with ammonia over Ag/Al_2O_3, Appl. Catal. B: Environ. 113-114 (2012) 228–236.
[20] D.E. Doronkin, T.S. Khan, T. Bligaard, S. Fogel, P. Gabrielsson, S. Dahl, Sulfur poisoning and regeneration of the Ag/gamma-Al_2O_3 catalyst for H_2-assisted SCR of NOx by ammonia, Appl. Catal. B-Environ. 117 (2012) 49–58.
[21] S. Fogel, D.E. Doronkin, P. Gabrielsson, S. Dahl, Optimisation of Ag loading and alumina characteristics to give sulphur-tolerant Ag/Al_2O_3 catalyst for H_2-assisted NH_3-SCR of NOx, Appl. Catal. B: Environ. 125 (2012) 457–464.
[22] P.S. Kim, M.K. Kim, B.K. Cho, I.-S. Nam, Autocatalytic synergism observed during lean-NOx reduction with a bifunctional reductant over Ag/Al_2O_3 catalyst, J. Catal. 292 (2012) 44–52.
[23] S. Tamm, S. Fogel, P. Gabrielsson, M. Skoglundh, L. Olsson, The effect of the gas composition on hydrogen-assisted NH_3-SCR over Ag/Al_2O_3, Appl. Catal. B: Environ. 136-137 (2013) 168–176.
[24] S. Tamm, N. Vallim, M. Skoglundh, L. Olsson, The influence of hydrogen on the stability of nitrates during H_2-assisted SCR over Ag/Al_2O_3 catalysts – A DRIFT study, J. Catal. 307 (2013) 153–161.
[25] D.E. Doronkin, S. Fogel, P. Gabrielsson, J.-D. Grunwaldt, S. Dahl, Ti and Si doping as a way to increase low temperature activity of sulfated Ag/Al_2O_3 in H_2-assisted NH_3-SCR of NOx, Appl. Catal. B: Environ. 148-149 (2014) 62–69.
[26] S. Fogel, P. Gabrielsson, H_2-assisted NH_3-SCR over Ag/Al_2O_3: An engine-bench study, Appl. Catal. B-Environ. 158 (2014) 1–10.
[27] W. Wang, J.M. Herreros, A. Tsolakis, A.P.E. York, Increased NO_2 concentration in the diesel engine exhaust for improved Ag/Al_2O_3 catalyst NH_3-SCR activity, Chem. Eng. J. 270 (2015) 582–589.
[28] X.Y. Wang, L.L. Jiang, J.Y. Wang, R.H. Wang, Ag/bauxite catalysts: Improved low-temperature activity and SO_2 tolerance for H_2-promoted NH_3-SCR of NOx, Appl. Catal. B-Environ. 165 (2015) 700–705.
[29] G. Xu, J. Ma, L. Wang, Z. Lv, S. Wang, Y. Yu, H. He, Mechanism of the H_2 effect on NH_3-selective catalytic reduction over Ag/Al_2O_3: Kinetic and diffuse reflectance infrared Fourier transform spectroscopy studies, ACS Catal. 9 (2019) 10489–10498.
[30] A. Marberger, D. Ferri, M. Elsener, O. Krocher, The significance of Lewis acid sites for the selective catalytic reduction of nitric oxide on vanadium-based catalysts, Angew. Chem. Int. Edit. 55 (2016) 11989–11994.
[31] G. He, Z. Lian, Y. Yu, Y. Yang, K. Liu, X. Shi, Z. Yan, W. Shan, H. He, Polymeric vanadyl species determine the low-temperature activity of V-based catalysts for the SCR of NOx with NH_3, Sci. Adv. 4 (11) (2018) eaau4637, https://doi.org/10.1126/sciadv.aau4637.
[32] G. Xu, J. Ma, L. Wang, W. Xie, J. Liu, Y. Yu, H. He, Insight into the origin of sulfur tolerance of Ag/Al_2O_3 in the H_2-C_3H_6-SCR of NOx, Appl. Catal. B: Environ. 244 (2019) 909–918.
[33] G. Xu, Y. Yu, H. He, A Low-Temperature Route Triggered by Water Vapor during the Ethanol-SCR of NOx over Ag/Al_2O_3, ACS Catal. 8 (4) (2018) 2699–2708.
[34] G. Xu, Y. Yu, H. He, Silver Valence State Determines the Water Tolerance of Ag/Al_2O_3 for the H_2–C_3H_6–SCR of NOx, J. Phys. Chem. C 122 (1) (2018) 670–680.
[35] G. Kresse, J. Furthmüller, Efficiency of ab-initio total energy calculations for metals and semiconductors using a plane-wave basis set, Computational Materials Science 6 (1) (1996) 15–50.
[36] M. Digne, P. Sautet, P. Raybaud, P. Euzen, H. Toulhoat, Hydroxyl groups on gamma-alumina surfaces: A DFT study, J. Catal. 211 (2002) 1–5.
[37] M. Digne, P. Sautet, P. Raybaud, P. Euzen, H. Toulhoat, Use of DFT to achieve a rational understanding of acid-basic properties of gamma-alumina surfaces, J. Catal. 226 (2004) 54–68.
[38] H. Deng, Y.B. Yu, F.D. Liu, J.Z. Ma, Y. Zhang, H. He, Nature of Ag species on Ag/gamma-Al_2O_3: A combined experimental and theoretical study, ACS Catal. 4 (2014) 2776–2784.
[39] C. Jia, G. Zhang, W. Zhong, J. Jiang, A First-Principle Study of Synergized O 2 Activation and CO Oxidation by Ag Nanoparticles on TiO 2 (101) Support, ACS Appl. Mater. Interfaces 8 (16) (2016) 10315–10323.
[40] M.Y. Chen, J.E. Dyer, K.J. Li, D.A. Dixon, Prediction of structures and atomization energies of small silver clusters, $(Ag)_n$, n < 100, J. Phys. Chem. A 117 (2013) 8298–8313.
[41] G. Henkelman, B.P. Uberuaga, H. Jónsson, A climbing image nudged elastic band method for finding saddle points and minimum energy paths, The Journal of Chemical Physics 113 (22) (2000) 9901–9904.
[42] G. Xu, J. Ma, G. He, Y. Yu, H. He, An alumina-supported silver catalyst with high water tolerance for H_2 assisted C_3H_6-SCR of NOx, Appl. Catal. B: Environ. 207 (2017) 60–71.
[43] D.Y. Yoon, J.-H. Park, H.-C. Kang, P.S. Kim, I.-S. Nam, G.K. Yeo, J.K. Kil, M.-S. Cha, DeNOx performance of Ag/Al_2O_3 catalyst by n-dodecane: Effect of calcination temperature, Appl. Catal. B: Environ. 101 (3–4) (2011) 275–282.
[44] P.S. Kim, M.K. Kim, B.K. Cho, I.S. Nam, S.H. Oh, Effect of H_2 on deNOx performance of HC-SCR over Ag/Al_2O_3: Morphological, chemical, and kinetic changes, J. Catal. 301 (2013) 65–76.
[45] M.K. Kim, P.S. Kim, J.H. Baik, I.-S. Nam, B.K. Cho, S.H. Oh, DeNOx performance of Ag/Al_2O_3 catalyst using simulated diesel fuel–ethanol mixture as reductant, Appl. Catal. B: Environ. 105 (1–2) (2011) 1–14.
[46] H. Kannisto, M. Skoglundh, K. Arve, E. Olsson, H. Härelind, Direct observation of atomically-resolved silver species on a silver alumina catalyst active for selective catalytic reduction of nitrogen oxides, Catal. Sci. Technol. 9 (22) (2019) 6213–6216.